Compact Modelling of Resistive Switching Devices based on the Valence Change Mechanism

Camilla La Torre
Instutitut für Werkstoffe der
Elektrotechnik II, RWTH Aachen
University & JARA-FIT
Aachen, Germany
latorre@iwe.rwth-aachen.de

Alexander F. Zurhelle
Instutitut für Werkstoffe der
Elektrotechnik II, RWTH Aachen
University & JARA-FIT
Aachen, Germany
a.zurhelle@iwe.rwth-aachen.de

Stephan Menzel
Peter Grünberg Institut (PGI-7)
Forschungszentrum Juelich GmbH &
JARA-FIT
Juelich, Germany
st.menzel@fz-juelich.de

Abstract—In this paper, a compact model for filamentary, resistive switching devices based on the valence change mechanism is proposed. It is based on the motion of ionic defects in a filamentary region. In contrast to previous model, it uses two state variables representing the ionic defect concentration close to the two opposing electrodes. This enables the modelling of ionic diffusion and, hence, drift–diffusion equilibria. In addition, the model can be used to simulate complementary switching in addition to the standard bipolar switching behavior.

Keywords—ReRAM, complementary switching, modelling, valence change mechanism

I. INTRODUCTION

Nonvolatile resistive switching devices based on the valence change mechanism (VCM) are a promising candidate for data storage, neuromorphic computing or computation-in-memory applications [1, 2]. By the application of appropriate voltage stimuli, VCM devices can be switched between at least two resistance states: a high resistive state (HRS) and a low resistive state (LRS). The switching mechanism relies on the non-isothermal drift and diffusion of ionic defects, typically oxygen vacancies, within a filamentary region of the oxide [3]. The change of the atomic configuration modulates the electrostatic barriers at the metal/oxide interfaces leading to a change in the local conductivity [3, 4]. To model this complex physical behavior, Marchewka and co-workers developed a physical continuum model. The simulation results show, for example, that the gradual RESET transition originates from the drift and diffusion of the ionic defects approaching a dynamic equilibrium [5, 6]. In addition, the transition from bipolar to complementary switching is related to the symmetrization of the electrostatic barriers at the opposing metal/oxide interfaces [7].

The rather long simulation times of continuum models, however, are not suited for circuit simulations. Thus, compact models need to be developed that allow for fast computation while still reproducing the experimental behavior. The compact models proposed in literature often use one state variable and only consider ionic drift [8-10]. These models can reproduce, for example, the nonlinear switching kinetics of VCM devices, but cannot account for a RESET equilibrium or complementary switching.

In this paper, we present a compact model that is capable of simulating the RESET equilibrium as well as complementary switching. The compact model is consistent with the results of our VCM continuum model [5, 6].
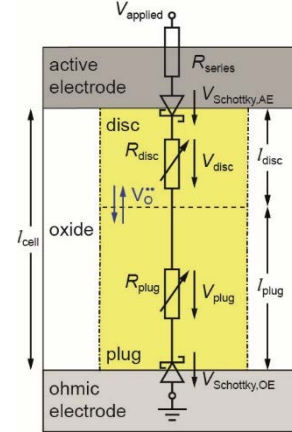

Fig. 1. Equivalent circuit diagram representing the electrical model of an asymmetric ReRAM device. The voltage is applied to the active electrode (AE), whereas the ohmic electrode (OE) is grounded.

The compact model is a part of our Juelich-Aachen Resistive Switching Tools (JART) and is called JART VCM v2.

II. SIMULATION MODEL

In the JART VCM v2 model, a filamentary region within the oxide matrix is considered as shown in Fig. 1a. The filamentary region of length l_{cell} is divided into two regions: the disc region and the plug region of length l_{disc} and l_{plug}, respectively. To each of these regions, one state variable is assigned, N_{disc} and N_{plug}, which represents the ionic defect concentrations (typically oxygen vacancies) in the disc and the plug, respectively. For each of these state variables one ordinary differential equation (ODE) is solved resulting in the coupled ODEs

$$\frac{dN_{disc}}{dt} = -\frac{1}{z_{Vo}\,e\,A\,l_{disc}} \cdot I_{ion} \qquad (1)$$

and

$$\frac{dN_{plug}}{dt} = \frac{1}{z_{Vo}\,e\,A\,l_{plug}} \cdot I_{ion}, \qquad (2)$$

where A is the cross-section of the filament, e is the elementary charge, and z_{Vo} is the charge number of the ionic defects. The change of the defect concentrations is proportional to the ionic current I_{ion}. As the increase/decrease of the disc and the plug concentration are interchanged in this model, the signs in eqs. (1) and (2) are opposite to each other. Thus, the total number of ionic defects in the whole filament stays constant during switching. The two state variables allow

TABLE I
SIMULATION PARAMETERS

Symbol	Value	Symbol	Value
l_{cell}	5 nm	$e\phi_{Bn0,AE}$	0.5 eV
l_{disc}	1.5 nm	$e\phi_{Bn0,OE}$	0.1 eV
l_{plug}	$l_{cell} - l_{disc}$	A^*	$6.01 \cdot 10^5$ A/(m^{2}K^2)
r_{fil}	35 nm	μ_{n0}	$5 \cdot 10^{-6}$ m^2/(Vs)
z_{Vo}	2	ΔE_{ac}	0.05 eV
a	0.4 nm	N_{max}	$6 \cdot 10^{27}$ m^{-3}
ν_0	$8 \cdot 10^{12}$ Hz	N_{min}	$1/(A \cdot l_{disc})$
ΔW_A	0.9 eV	$R_{series,0}$	1200 Ω
ε	$17 \cdot \varepsilon_0$	$R_{th,eff}$	$1.6 \cdot 10^6$ K/W
ε_{ϕ_B}	$5.5 \cdot \varepsilon_0$	T_0	293 K

us to model the ionic diffusion current density $J_{ion,diffusion}$ between these two regions, in addition to the ionic drift current density $J_{ion,drift}$ according to

$$I_{ion} = A\left(J_{ion,drift} + J_{ion,diffusion}\right)$$
$$= A\left(CN\sinh\left(\frac{a\,z_{Vo}eE}{2\,k_B T}\right)\cdot F_{limit} - C\frac{a}{2}\frac{dN}{dx}\cosh\left(\frac{a\,z_{Vo}eE}{2\,k_B T}\right)\right), \quad (3)$$

with

$$C = 2z_{Vo}e\,a\,\nu_0 \exp\left(-\frac{\Delta W_A}{k_B T}\left[\sqrt{1-\gamma^2} + \gamma\arcsin\gamma\right]\right), \quad (4)$$

and

$$\gamma = \frac{a\,z_{Vo}eE}{\pi\Delta W_A}. \quad (5)$$

In eqs. (3)-(5), a is the hopping distance, k_B is the Boltzmann constant, ΔW_A is the migration barrier, and ν_0 is the attempt frequency for ion hopping. The function F_{limit} is introduced to prevent unreasonable defect concentrations and keep them between a maximum N_{max} and minimum concentration N_{min} [11]. The concentration gradient in eq. (3) is defined according to

$$\frac{dN}{dx} = \frac{N_{plug} - N_{disc}}{0.5\,l_{cell}}. \quad (6)$$

Furthermore, the mean concentration N in eq. (3) is calculated using

$$N = \sqrt{N_{disc}\cdot N_{plug}}. \quad (7)$$

The ionic current depends in a nonlinear manner on the electric field E. In principle, the electric field varies along the filament due to different work functions and space charge effects. This complex space-dependency needs to be approximated for compact modelling. If the work functions of the two metals are identical, the length of disc and plug are considered to be identical. In this symmetric case, the electric field is defined as

$$E_{symmetric} = \frac{V_{disc} + V_{plug}}{l_{cell}}, \quad (8)$$

where V_{disc} (V_{plug}) defines the voltage drop over the disc (plug) region. For differing work functions and lengths, the band bending under forward and reverse bias of the disc/metal interface is different. Thus, the definition of the electric field becomes polarity-dependent and

$$E_{asymmetric} = \begin{cases} \dfrac{V_{disc} + V_{plug}}{l_{cell}} & V_{applied} > 0 \text{ (RESET)} \\[2ex] \dfrac{V_{disc}}{l_{disc}} & V_{applied} < 0 \text{ (SET)} \end{cases} \quad (9)$$

is used. Here, it is always assumed that the disc is close to the electrode with the higher work function, which is called active electrode (AE). The electrode close to the plug region is called ohmic electrode (OE) as it shows a very small interface barrier.

The ionic current depends on the filament temperature T, which can increase from the ambient temperature T_0 due to local Joule heating. Thus, the temperature becomes a function of the dissipated electrical power and it is approximated by

$$T = (V_{disc} + V_{plug})\cdot I\cdot R_{th,eff} + T_0. \quad (10)$$

In eq. (10), $R_{th,eff}$ is the equivalent thermal resistance of the device. It represents the heat dissipation via the electrodes and the surrounding material. The total current flowing through the cell (the filament) is determined using the equivalent circuit diagram in Fig. 1. The two "Schottky" contacts are modelled by assuming thermionic field emission I_{TFE} and thermionic emission I_{TE} in reverse and forward direction of the contact, respectively. As the two "Schottky" contacts have opposite polarities, a signum function needs to be used in the calculation of the current as

$$I = \begin{cases} \text{sign}(V_{applied})\cdot I_{TE} & V_{Schottky} > 0 \text{ (forward)} \\ \text{sign}(V_{applied})\cdot I_{TFE} & V_{Schottky} > 0 \text{ (reverse)} \end{cases}. \quad (11)$$

Thus, while one Schottky contact is biased in forward direction the other one is biased in reverse direction. The currents are strongly nonlinear dependent on the ionic defect concentration close to the respective contacts. If the defect concentration increases, the current increases, too. The disc (plug) resistance R_{disc} (R_{plug}) is also a function of the disc (plug) concentration and is calculated according to

$$R_{disc/plug} = \frac{l_{disc/plug}}{A\cdot z_{Vo}e\mu_{n0}N_{disc/plug}}\exp\left(\frac{\Delta E_{ac}}{k_B T}\right). \quad (12)$$

A band conduction mechanism with mobility μ_{n0} is assumed, in which the defect concentration defines the numbers of electrons in the conduction band. A slight temperature activation ΔE_{ac} of the transport is assumed as well. Further details of the model, like the used equations for F_{limit}, I_{TFE}, and $I_{TE,}$ can be found in [11]. The model has been implemented in MATLAB and Verilog-A. Both model implementations of the JART VCM v2 model can be downloaded from our web site [12]. The used simulation parameters are given in Table I.

III. SIMULATION RESULTS

In a first simulation, constant voltage pulses with different amplitudes are used to study the RESET transition. Here, we assume an asymmetric cell. Fig. 2a shows the simulated current transients for three different RESET voltage amplitudes. The transition starts first for the highest voltage amplitude and then the current decreases gradually. This current transition is caused by the change of the disc concentration due to the applied voltage (Fig. 2b). Eventually, the current does not change anymore. In the constant current regime, the disc concentration is constant, too. Thus, the disc concentration does not change anymore while the voltage is still applied.
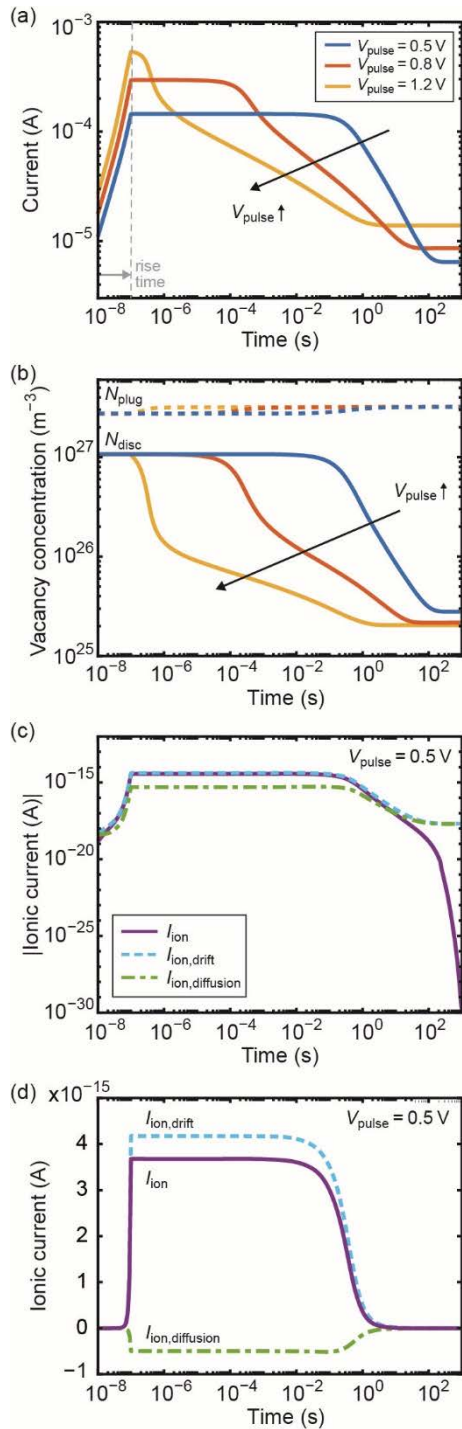
Fig. 2. For three RESET pulses (rise time 100 ns) with V_{pulse} = 0.5 V, V_{pulse} = 0.8 V, and V_{pulse} = 1.2 V, the current transients (a) and the oxygen vacancy concentrations in the plug and the disc (b) are compared. For the initial LRS, $N_{disc,initial}$ = 1.07·10^{27} m^{-3} and $N_{plug,initial}$ = 2.75·10^{27} m^{-3} are used. For V_{pulse} = 0.5 V, the total ionic current and its drift and diffusion component are plotted on (c) a logarithmic and (d) a linear scale.

As shown in Fig. 2c and d, the constant disc concentration originates from the approached equilibrium of drift and diffusion. During the RESET transition, the ionic drift moves the positively charged oxygen vacancies from the disc region to the plug region. Thus, a concentration gradient builds up, which gives rise to an ionic diffusion current counteracting the drift current. Eventually, these two currents reach an equilibrium. The simulation results also show that the final disc concentration is a function of the applied pulse voltage
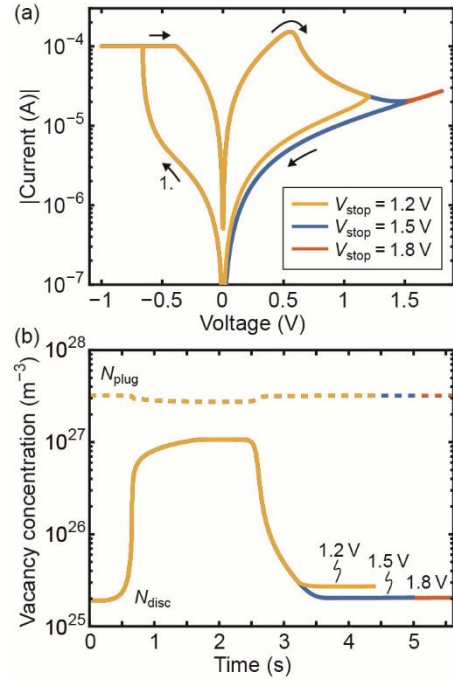

Fig. 3. Influence of V_{stop} on the HRS during the RESET and its limit. All sweeps are simulated with a sweep rate of 1 V/s. The initial HRS is defined by $N_{disc,initial}$ = 1.9·10^{25} m^{-3} and $N_{plug,initial}$ = 3.2·10^{27} m^{-3}. (a) I–V curves with a maximum positive sweep voltage of 1.2 V, 1.5 V, and 1.8 V, respectively. (b) Oxygen vacancy concentration in the plug and the disc for the three stop voltages.

V_{pulse}. The higher the pulse amplitude, the smaller is the final disc concentration. Thus, the final resistance is higher for a higher RESET voltage used. These results are equivalent to the results of our continuum model and consistent with experimental data [6]. In a second simulation study, the RESET equilibrium is investigated for voltage sweeps with varying RESET stop voltage V_{stop}. As shown in Fig. 3a, the increase of V_{stop} leads to different HRS, but at very high V_{stop}, the HRS stays constant. Similar to the constant voltage operation a drift–diffusion equilibrium evolves, which results in constant values for the disc and plug concentration (Fig. 3b). The tuning of the HRS with the RESET stop voltage has been reported for various VCM cells in literature [5, 13-16]. The occurrence of an HRS saturation has been reported as well [17, 18].

Besides the simulation of the RESET equilibrium, the JART VCM v2 model allows us to simulate complementary switching behavior. For the simulation results shown in Figs. 2 and 3, an asymmetric device structure is assumed as discussed before. The electrostatic barrier at the active electrode is a lot higher than the one at the ohmic electrode. In this case, N_{disc} determines the overall current through the device and thus the switching is bipolar. If a symmetric stack is considered, the lower one of the two concentrations will determine the overall current. In Fig. 4a, the concentration in the left half of the cell is lower. As long as the concentration on the left side is limited to lower values than on the right side due to the (chosen) current compliance, bipolar switching is obtained. If no current compliance is used, the ionic defects can move completely from the left region to the right region and vice versa. This leads to complementary switching behavior as shown in Fig. 4b. Figure 4c shows a bipolar switching mode, which results from the change of the concentration in the right region. This behavior is consistent with experimental data [19, 20] and our continuum model [7].
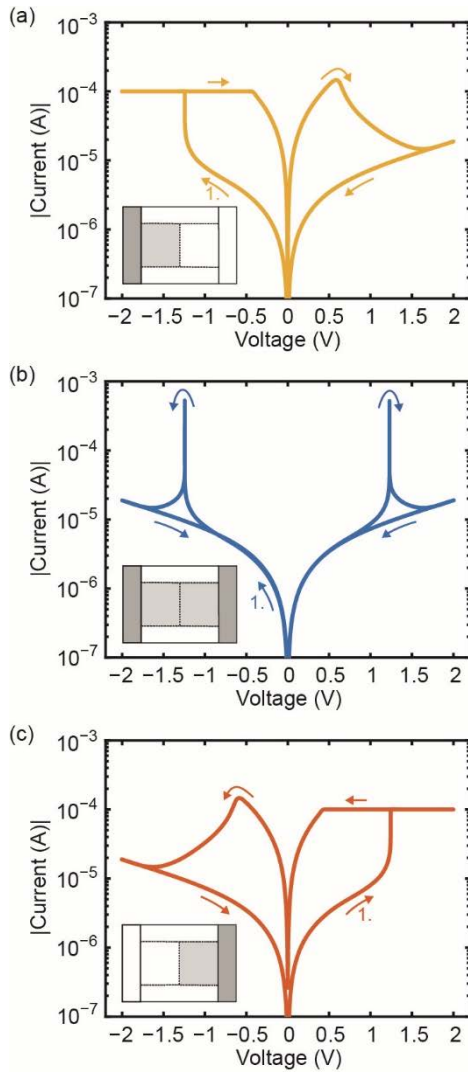
229

Fig. 4. Transition of bipolar and complementary switching. (a) Bipolar switching at one electrode by applying a current compliance for negative voltages. (b) Complementary switching arises in a symmetric model if no current compliance is active. (c) Bipolar switching at the other electrode by applying a current compliance for positive voltages. The initial values for the defect concentrations in both regions are similar to the simulation in Fig. 3. The device stack is symmetric with $l_{disc} = l_{plug} = 2.5$ ns and $e\phi_{Bn0,AE} = e\phi_{Bn0,OE} = 0.3$ eV.

IV. Conclusions

In this paper, we present a compact model that can simulate the RESET equilibrium and complementary switching behavior. To this end, a second state variable is introduced, which enables us to implement ionic diffusion in addition to ionic drift. The simulation results are consistent with our previous physical continuum model, but significantly reduce the simulation times.

Acknowledgment

References

[1] J. J. Yang, D. B. Strukov and D. R. Stewart, "Memristive Devices for Computing," *Nat. Nanotechnol.*, vol. 8, pp. 13-24, 2013.

[2] D. Ielmini and H. P. Wong, "In-memory computing with resistive switching devices," *Nature Electronics*, vol. 1, pp. 333-343, 2018.

[3] R. Waser, R. Dittmann, G. Staikov and K. Szot, "Redox-Based Resistive Switching Memories - Nanoionic Mechanisms, Prospects, and Challenges," *Adv. Mater.*, vol. 21, pp. 2632-2663, 2009.

[4] J. J. Yang, M. D. Pickett, X. Li, D. A. A. Ohlberg, D. R. Stewart and R. S. Williams, "Memristive switching mechanism for metal/oxide/metal nanodevices," *Nat. Nanotechnol.*, vol. 3, pp. 429-433, 2008.

[5] A. Marchewka, B. Roesgen, K. Skaja, H. Du, C. L. Jia, J. Mayer, V. Rana, R. Waser and S. Menzel, "Nanoionic Resistive Switching Memories: On the Physical Nature of the Dynamic Reset Process," *Adv. Electron. Mater.*, vol. 2, pp. 1500233/1-13, 2016.

[6] A. Marchewka, R. Waser and S. Menzel, "A 2D Axisymmetric Dynamic Drift-Diffusion Model for Numerical Simulation of Resistive Switching Phenomena in Metal Oxides," *2016 International Conference On Simulation of Semiconductor Processes and Devices (SISPAD), Nuremberg, Germany, September 6-8, 2016*, 2016, pp. 145-148.

[7] A. Marchewka, R. Waser and S. Menzel, "Physical Simulation of Dynamic Resistive Switching in Metal Oxides Using a Schottky Contact Barrier Model," *2015 International Conference On Simulation of Semiconductor Processes and Devices (SISPAD), 9-11 September, Washington D.C, USA*, 2015, pp. 297-300.

[8] Z. Jiang, Y. Wu, S. Yu, L. Yang, K. Song, Z. Karim and H.-P. Wong, "A Compact Model for Metal-Oxide Resistive Random Access Memory With Experiment Verification," *IEEE Trans. Electron Devices*, vol. 63, pp. 1884-1892, 2016.

[9] A. Hardtdegen, C. La Torre, F. Cüppers, S. Menzel, R. Waser and S. Hoffmann-Eifert, "Improved Switching Stability and the Effect of an Internal Series Resistor in HfO₂/TiOₓ Bilayer ReRAM Cells," *IEEE Trans. Electron Devices*, vol. 65, pp. 3229-3236, 2018.

[10] S. Ambrogio, S. Balatti, D. C. Gilmer and D. Ielmini, "Analytical Modeling of Oxide-Based Bipolar Resistive Memories and Complementary Resistive Switches," *IEEE Trans. Electron Devices*, vol. 61, pp. 2378-2386, 2014.

[11] C. La Torre, A. F. Zurhelle, T. Breuer, R. Waser and S. Menzel, "Compact Modeling of Complementary Switching in Oxide-Based ReRAM Devices," *IEEE Trans. Electron Devices*, vol. 66, pp. 1268-1275, 2019.

[12] JART, "Juelich Aachen Resistive Switching Tools (JART)," www.emrl.de/JART.html, 2019.

[13] W. Hu, L. Zou, C. Gao, Y. Guo and D. Bao, "High speed and multi-level resistive switching capability of Ta2O5 thin films for nonvolatile memory application," *J. Alloy. Compd.*, vol. 676, pp. 356-360, 2016.

[14] S. Yu, Y. Wu, R. Jeyasingh, D. Kuzum and H. P. Wong, "An Electronic Synapse Device Based on Metal Oxide Resistive Switching Memory for Neuromorphic Computation," *IEEE Trans. Electron Devices*, vol. 58, pp. 2729-2737, 2011.

[15] H. K. Li, T. P. Chen, S. G. Hu, P. Liu, Y. Liu, P. S. Lee, X. P. Wang, H. Y. Li and G. Q. Lo, "Study of Multilevel High-Resistance States in HfOₓ-Based Resistive Switching Random Access Memory by Impedance Spectroscopy," *IEEE Trans. Electron Devices*, vol. 62, pp. 2684-2688, 2015.

[16] F. Yuan, Z. Zhang, L. Pan and J. Xu, "A Combined Modulation of Set Current With Reset Voltage to Achieve 2-bit/cell Performance for Filament-Based RRAM," *IEEE J. Electron Devices Soc.*, vol. 2, pp. 154-157, 2014.

[17] J. Frascaroli, S. Brivio, E. Covi and S. Spiga, "Evidence of soft bound behaviour in analogue memristive devices for neuromorphic computing," *Sci Rep*, vol. 8, pp. 7178/1-12, 2018.

[18] L. Larcher, F. M. Puglisi, P. Pavan, A. Padovani, L. Vandelli and G. Bersuker, "A Compact Model of Program Window in HfOx RRAM Devices for Conductive Filament Characteristics Analysis," *IEEE Trans. Electron Devices*, vol. 61, pp. 2668-2673, 2014.

[19] F. Nardi, S. Balatti, S. Larentis, D.C. Gilmer and D. Ielmini, "Complementary Switching in Oxide-Based Bipolar Resistive-Switching Random Memory," *IEEE Trans. Electron Devices*, vol. 60, pp. 70-77, 2013.

[20] S. Balatti, S. Larentis, D. C. Gilmer and D. Ielmini, "Multiple Memory States in Resistive Switching Devices Through Controlled Size and Orientation of the Conductive Filament," *Advanced Materials*, vol. 25, pp. 1474-1478, 2013.